Swelling of Thick Polymer Brushes Investigated with Ellipsometry

Jörg Habicht, Markus Schmidt, Jürgen Rühe, and Diethelm Johannsmann*

Max-Planck-Institute for Polymer Research, Ackermannweg 10, 55128 Mainz, Germany

Received May 13, 1998. In Final Form: December 21, 1998

We have investigated the swelling of a polystyrene brush in cyclohexane at varying temperatures with angle-dependent ellipsometry. The brush was grown in situ on the base of a high index prism by the "grafting from" technique. In the dry state it has a thickness of $d = 134$ nm. At the θ temperature it swells to about 600 nm. In accordance with the predictions from mean field theory, the brush thickness continuously increases with solvent quality. As the thickness increases, the shape of the segment density profile becomes smoother with a broad dilute transition region between the brush and the solvent.

Introduction

Tethered polymer layers have recently attracted a lot of scientific interest in both fundamental science and application-oriented research.[1−7] The covalent terminal attachment to the substrate prevents desorption and dewetting even under good solvent conditions. It leads to conformations and dynamics which are significantly different from the behavior of bulk polymers. Polymer-tethered layers are widely used for the purpose of colloid stabilization.[8] Other applications such as adhesion,[9] lubrication,[10] tribology,[11] chromatography,[12] and rheology[13] have also been put forward.

In good solvents tethered layers swell. The thickness of the swollen layers is governed by the balance between osmotic pressure and chain stretching. In polymer brushes, where the grafting distance is less than the dimension of the unperturbed chain, chain crowding enters as a new distinctive feature. The osmotic pressure strongly depends on solvent quality. Various works employing analytical theory[14,15] simulation,[16] and neutron reflection[17] have shown that the brush collapse with decreasing solvent quality proceeds continuously. This gradual collapse contrasts with the behavior of bulk polymers of high molecular weight which discontinuously phase separate into a dense and a dilute phase just below the θ point.[18,19] Isolated polymer chains also change their conformation from Gaussian chains ($R_g \sim N^{1/2}$) to globular spheres ($R_g \sim N^{1/3}$) just below the θ condition.[20] In brushes the collapse is smoothened due to the constraints imposed by the grafting.

Most of the previous investigations have been carried out on brushes prepared either by surface adsorption of block copolymers[21−23] or by chemically grafting polymer chains to the substrate.[17] In both cases the thickness of the brush is rather limited, because during the process of brush formation the polymer chains already attached to the surface act as a diffusion barrier for subsequent further adsorption of other polymer chains from the bulk. The ratio of thickness and grafting density (the number of blobs in the De Gennes picture[2]) rarely exceeds 20.[17] This statement holds regardless of the molecular weight of the adsorbed chains. If short chains are adsorbed, the graft density can be increased, but this happens at the expense of chain length, which again limits the ratio of thickness to graft distance.

We have recently established a new method to prepare polymer brushes in which the polymer chains are grown in situ on the solid surface[24,25] (Figure 1). The brush growth occurs via radical polymerization from an initiator which has been covalently attached to the surface. In contrast to conventional grafting procedures, the rate-limiting step is the diffusion of monomers toward the growing chain end rather than polymer diffusion. To emphasize the conceptual difference, the method has been termed "grafting from". By in situ growing the polymer chains, brush thicknesses of 900 nm in the dry state have been achieved for polystyrene on gold.[26] A typical distance

* To whom correspondence should be addressed. Phone: 49-6131-379 163. Fax: 49-6131-379 360. E-mail: johannsmann@mpip-mainz.mpg.de.

(1) Alexander, S. *J. Phys. (Paris)* **1977**, *38*, 983.
(2) de Gennes, P. G. *J. Phys. (Paris)* **1976**, *37*, 1443.
(3) Halperin, A.; Tirell, M.; Lodge, T. P. *Adv. Polym. Sci.* **1991**, *100*, 31.
(4) Halperin, A. In *Soft Order in Physical Systems*, Vol. 323 of Series B: Physics; Rabin, Y., Bruinsma, R., Eds.; Plenum Press: New York, 1994; pp 33−56.
(5) Szleifer, I.; Cariggnano, M. A. *Adv. Chem. Phys.* **1996**, *XCIV*, 165.
(6) Grest, G. S.; Murat, M. In *Monte Carlo and Molecular Dynamics Simulations in Polymer Science*; Binder, K., Ed.; Clarendon Press: Oxford, 1994.
(7) Milner, S. T. *Science* **1991**, *251*, 905.
(8) Napper, D. H. *Steric Stabilization of Colloidal Dispersions*; Academic Press: New York, 1983.
(9) Raphaël, E.; de Gennes, P. G. *J. Phys. Chem.* **1992**, *96*, 4002.
(10) Klein, J. *Annu. Rev. Mater. Sci.* **1996**, *26*, 581.
(11) Klein, J.; Kumacheva, E. *Science* **1995**, *269*, 816.
(12) van Zanten, J. H. *Macromolecules* **1994**, *27*, 6797.
(13) Parnas, R. S.; Cohen, Y. *Rheol. Acta* **1994**, *33*, 485.
(14) Halperin, A. *J. Phys. (Paris)* **1988**, *49*, 547.
(15) Zhulina, E. B.; Borisov, O. V.; Pryamitsyn, V. A.; Birshtein, T. M. *Macromolecules* **1991**, *24*, 140.
(16) Grest, G. S.; Murat, M. *Macromolecules* **1993**, *26*, 3108.
(17) Karim, A.; Satija, S. K.; Douglas, J. F.; Ankner, J. F.; Fetters, L. J. *Phys. Rev. Lett.* **1994**, *73*, 3407.
(18) Daoud, M.; Jannink, G. *J. Phys. (Paris)* **1976**, *37*, 973.
(19) Einaga, Y.; Tong, Z.; Fujita, H. *Macromolecules* **1985**, *18*, 2258.
(20) de Gennes, P. G. *Scaling Concepts in Polymer Physics*; Cornell University Press: Ithaca, NY 1979.
(21) Field, J. B.; Toprakcioglu, C.; Ball, R. C.; Stanley, H. B.; Dai, L.; Barford, W.; Penfold, J.; Smith, G.; Hamilton, W. *Macromolecules* **1992**, *25*, 434.
(22) Tirell, M. In *Solvents and Self-Organization of Polymers*; Kluwer Academic Publishers: Dordrecht, 1996.
(23) Webber, R. M.; van der Linden, C. C.; Anderson, J. L. *Langmuir* **1996**, *12*, 1040.
(24) Prucker, O.; Rühe, J. *Macromolecules* **1998**, *31*, 592.
(25) Prucker, O.; Rühe, J. *Macromolecules* **1998**, *31*, 602.

10.1021/la980573d CCC: $18.00
Published on Web 03/12/1999

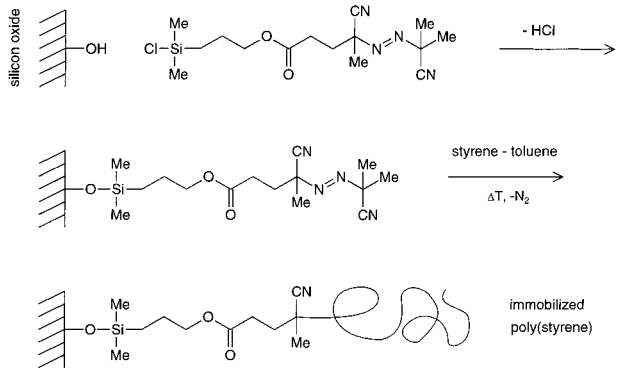

Figure 1. Synthesis of tethered polymer layers by the "grafting from" approach. The initiator is self-assembled on a silicon oxide surface. The polymer grows in situ by free radical polymerization from the surface-bound initiator.

between two grafting sites is 2−3 nm. The molecular weight can be has high as 10^6 g/mol with a polydispersity of $M_w/M_n \sim 2$. The polydispersity is larger than for most brushes attached by "grafting to" because free radical polymerization is employed. With regard to a test of the theoretical pictures the large polydispersity certainly is a disadvantage.[27] However, in practical application many tethered chain systems used for steric stabilization of polymeric latices are generated in a similar way and are therefore highly polydisperse as well.

For brushes obtained by "grafting from" chain stretching is obtained even in the dry state. The dry thickness of the brush investigated here is 134 nm, which corresponds to about 2 radii of gyration of the unperturbed chain. The number of blobs given by the ratio of brush thickness and grafting distance is about 50 in the dry state. During swelling it increases to more than 200.

The collapse of the brush under varying solvent conditions is conveniently measured for the polystyrene/cyclohexane system, where the solvent quality can be adjusted via temperature. In the bulk the θ point is at 34 °C.[28] Shorter polystyrene brushes in cyclohexane (CH) have been previously investigated with neutron reflectometry by Karim and co-workers.[17] It was found that the mean field description adequately describes the collapse. Polystyrene tethered layers adsorbed to micropores have been investigated with regard to their hydrodynamic thickness by Webber and co-workers.[23] In this case the hydrodynamic thickness increased more strongly with solvent quality than predicted by mean-field theory. Here we report on an optical investigation on a thick brush prepared by "grafting from". Since the brush thickness is comparable to the wavelength of light, it can be measured with variable-angle ellipsometry. Most of the information is contained in the region of oblique incidence. To access this range of incidence angles, we grew the brush directly on the base of a high-index prism and measured the ellipsometric parameters $\psi(\theta)$ and $\Delta(\theta)$ both below and above the critical angle (Figure 2). The evanescent part of the ellipsometric spectrum contains very valuable additional information, as well.

Materials

The synthesis of the polymer brush followed the "grafting from" approach[24,25] as depicted in Figure 1. Briefly, the first step is the formation of a self-assembled monolayer of an initiator for free radical polymerization at the surface of a high index LaSFN9 prism. The prism was pretreated for 5 min with 1 M sulfuric acid to activate the surface hydroxyl groups. The initiator used was a derivative of AIBN which is attached to the glass surface via a monochlorosilyl moiety. Subsequently, the polymerization was thermally initiated in bulk styrene monomer. After polymerizing for 24 h at 60 °C, the sample was rinsed with solvent and underwent Soxhlet extraction with toluene for 15 h to remove physisorbed polymer. In the dry state the brush was 134 nm thick as determined by null ellipsometry. The molecular weight is a priori unknown. However, one can infer the molecular weight from reference experiments on large substrates. In these cases the grafted polymer was cleaved off the surface by acid-catalyzed transesterification of an ester break-seal incorporated into the initiator molecule (cf. Figure 1). This material was investigated with size exclusion chromatography and static light scattering. For the sample investigated here the estimated molecular weight is $M_n \sim 500\,000-1\,000\,000$ g/mol. The polydispersity is in the range of $M_w/M_n \sim 2$. From the thickness and the molecular weight the distance between two grafting sites is estimated as 2−3 nm.

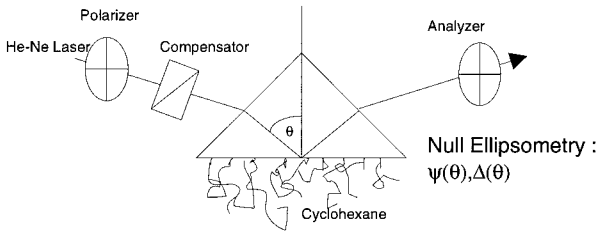

Figure 2. Schematic drawing of the experimental setup. The brush is not drawn to scale.

Experimental Procedure and Data Analysis. Figure 2 shows a sketch of the experimental setup. We used a home-built, variable-angle null-ellipsometer.[29] The light source is a He−Ne laser with a wavelength $\lambda = 633$ nm. Polystyrene is perfectly transparent at this wavelength. The sample is grown on an LaSFN9 prism with a refractive index of $n = 1.845$. In contact with cyclohexane the critical angle of total reflection is between 50.025° (45 °C) and 50.535° (15 °C). Above the critical angle the optical field evanescently decays into the bulk. The main features used for analysis occur close to the critical angle, where the inverse wave vector q_z^{-1} matches the brush thickness. Below the critical angle q_z^{-1} corresponds to $\lambda/\cos\theta$ with λ the wavelength and θ the direction of the light beam. For evanescent waves q_z^{-1} is imaginary and corresponds to the decay length of the evanescent field.

The laser spot was clearly visible on the sample, which indicates some scattering and lateral heterogeneities. Heterogeneities are also evidenced by the substantial residual intensity at the detector obtained after optimizing the polarizer and analyzer position for minimum throughput. This depolarization is caused by small angle scattering. The largest residual intensity is observed close to the critical angle θ_c. Close to θ_c, one observes a halo of scattered light around the specularly reflected beam. Small angle scattering is strongest close to θ_c because under this condition the small scattering vectors lie in the sample plane. Because of the large depolarization we excluded a range of ±0.6° around the critical angle for the lower temperatures and +0.6° above the critical angle for the higher temperatures from the fitting procedure.

To further address the issue of lateral heterogeneity, we investigated the sample with imaging ellipsometry.[30,31] Figure 3 shows a typical picture. One observes a considerable amount of lateral structure. These heterogeneities are somewhat surprising because brushes prepared on silicon wafers usually look smooth both in the optical microscope and under the scanning

(26) Habicht, J.; Rühe, J. In preparation.
(27) Milner, S. T.; Witten, T. A.; Cates, M. E. *Macromolecules* **1989**, *22*, 853.
(28) Strazielle, C.; Benoit, H. *Macromolecules* **1975**, *8*, 203.
(29) Azzam, R. M. A.; Bashara, N. M. *Ellipsometry and Polarized Light*; Elsevier: Amsterdam, 1987.
(30) Stenberg, M.; Sandström, T.; Stilbert, L. *Mater. Sci. Eng.* **1980**, *42*, 65.
(31) Reiter, R.; Motschmann, H.; Orendi, H.; Nemetz, A.; Knoll, W. *Langmuir* **1992**, *8*, 1784.

Figure 3. Micrograph of the sample taken with imaging ellipsometry. Presumably, the observed patterns are remanents from the polishing process which have been amplified by the chemical activation process prior to the growth of the brush. The size of the image is about 0.5 × 0.7 mm.

force microscope. At this point we can only speculate about the origin of the heterogeneities. Possibly, the activation process with sulfuric acid prior to the self-assembly of the azo-initiator has etched the prism surface. The features seen in Figure 3 resemble traces from polishing, which may have been amplified by the etching process. In particular the heterogeneities do not appear intrinsic in the sense that they originate from fluctuations of the brush profile such as breathing modes or octopus micelles discussed in the literature.[32−35] Octopus micelles, in particular, are not even expected because the grafting density is very high.

Although the prism was mounted very gently, some residual stress birefringence could not be avoided. Ideally, the parameter Δ should be 0° or 180° for a flat dielectric interface below the critical angle. Due to residual birefringence, this is not the case in our experiments. In reference experiments with a bare prism in contact with cyclohexane, we observed a discrepancy between theory and experimental data of up to 6°. The data analysis relies on features of the ellipsometric spectrum rather than on absolute values. We therefore allowed for an offset in Δ in the fitting routine. For the parameter ψ the discrepancies were less severe.

The refractive index profile is inferred from the angle dependence of the complex reflectivities r_p and r_s for p- and s-light.[29] The ellipsometric parameter tan(ψ) is the modulus of the ratio r_p/r_s; the parameter Δ is the phase difference. The fit results shown as straight lines in Figure 3 were obtained with complementary error functions

$$\varphi_p(z) = \varphi_0 \frac{1}{2}\left[1 - \mathrm{erf}\left(\frac{z-d}{w}\right)\right] \qquad (1)$$

with φ_p the polymer volume fraction, d the thickness, w the

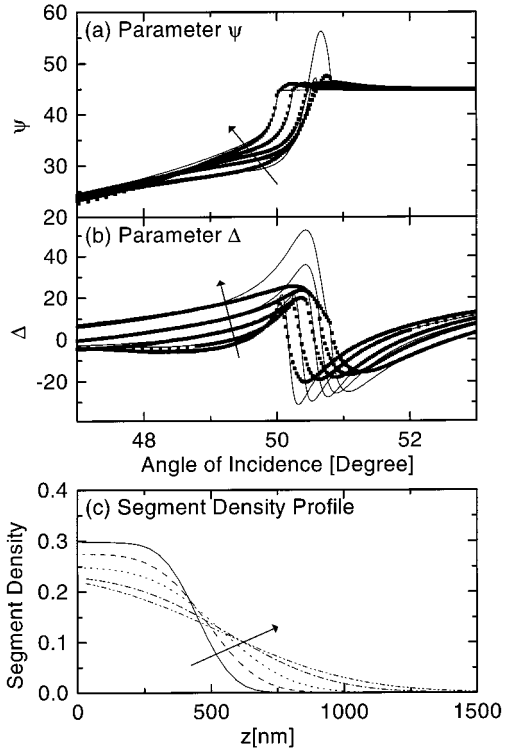

Figure 4. Ellipsometric parameters ψ (a) and Δ (b) for $T = 15$, 23, 30, 38, and 45 °C. Part c shows the segment density profiles according to the best fits. The arrows indicate increasing temperatures.

"interface width", and φ_0 a normalization constant. The parameter w quantifies to what extent the profile is boxlike or not. A large parameter w corresponds to a smooth profile with a large region of dilute polymer slowly decaying in concentration as the distance from the surface gets larger. For numerical calculation the profile was cut into 50 slabs with constant refractive index; i.e., the error function was approximated by a succession of steps. The cutoff at high z was set such that it was more than $4w$ away from the point of inflection ($z = d$). On selected data sets we performed tests with higher cutoff distances and a larger number of slabs and did not find significant differences. The ellipsometric parameters ψ and Δ were calculated from these stepwise constant profiles according to the matrix method. Since the matrix method is based on a complex formalism, it works for propagating waves (q_z real) and evanescent waves (q_z imaginary) in essentially the same way.

For simplicity, we assumed that the refractive index is a linear function of the polymer volume fraction, i.e., that $dn/d\varphi_p$ = constant = $n_{PS} - n_{CH}$. The temperature dependence of the refractive index of cyclohexane dn_{CH}/dT was measured in a Michelson interferometer setup as $dn/dT = -5.54 \times 10^{-4}$ °C^{-1}. This was in agreement with the observed critical angles. In fact, a careful measurement of the critical angle was the most reliable way to measure the temperature at the sample. The temperature dependence of the prism's refractive index is negligible.

Figure 4 shows the data sets and fits obtained at the temperatures T = 15, 23, 30, 38, and 45 °C. Evidently, there remains some systematic discrepancy between the fits and the data. Given the lateral heterogeneities as evidenced from microscopy, we have not attempted to improve the quality of the fits with more complicated fit functions. In particular, we find it quite plausible that the sharp features in the fits appear smoothened out in the experiment. The influence of heterogeneities is largest for steep profiles which occur at low temperatures and less severe at the higher temperatures where the profiles are smoother.

Even for perfectly homogeneous samples, it is not expected that fine details of the segment density profile can be resolved with ellipsometry because of the long wavelength of light. We

(32) Yeung, C.; Balazs, A. C.; Jasnow, D. *Macromolecules* **1993**, *26*, 1914.
(33) Lai, P.-Y.; Binder, K. *J. Chem. Phys.* **1992**, *97*, 586.
(34) Fytas, G.; Anastasiadis, S. H.; Seghrouchni, R.; Vlassopoulos, D.; Li, J.; Factor, B. J.; Theobald, W.; Toprakcioglu, C. *Science* **1996**, *274*, 2041.
(35) Zhulina, E. B.; Birshtein, T. M.; Priamitsyn, V. A.; Klushin, L. I. *Macromolecules* **1995**, *28*, 8612.

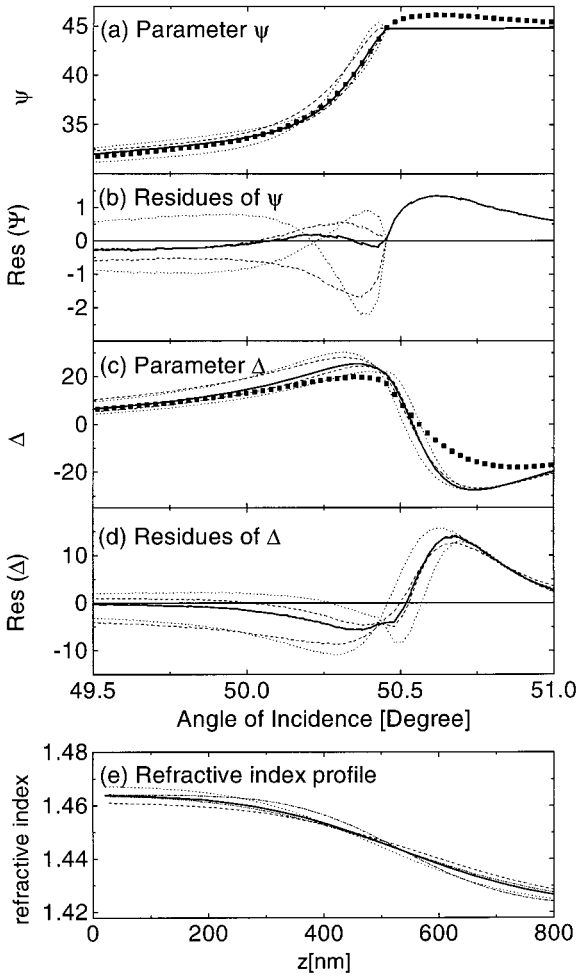

Figure 5. Comparison of the best fit (straight line) and fits which were considered to marginally acceptable (dashed and dotted lines). From fit parameters corresponding to the dashed and dotted lines, the error bars in Figure 6 were generated.

have chosen error functions as fit functions because they are the simplest functions compatible with what one qualitatively expects for polymer brushes. Also, they are in agreement with recent results on shorter polystyrene brushes under bad to moderate solvent conditions obtained by neutron reflectivity.[36] Parabolic profiles should not correctly describe the profile because of polydispersity.[37] From the error functions we extract the parameters d and w, which are measures of the brush thickness and the interface width. The parameters d and w are related to the first and the second moments of the segment density profile.

In Figure 5 we demonstrate for the data set at $T = 30$ °C that both the thickness d and the interface width w are reliably determined from fitting. The solid squares are the experimental data. Just above the critical angle the scattering is largest. As usual, the scattering is stronger for s- light than for p-light. The parameter ψ therefore is higher than 45°. We excluded a range of 0.6 ° above the critical angle from the fit. The thick straight line is the best fit. The two dotted lines are fits where the thickness d has been changed by +30 and −30 nm; the two dashed lines are fits where the interface width w has been changed by +50 and −50 nm. Changes in d shift the features in the Δ-plot on the horizontal scale (parts c and d of Figure 5). Changes in w mainly affect the curvature of $\psi(\theta)$ below the critical angle (parts a and b of Figure 5). For $T = 30$ °C we estimate $\Delta w = \pm 30$ nm and $\Delta d = \pm 50$ nm.

(36) Bunjes, N.; Paul, S.; Habicht, J.; Prucker, O.; Rühe, J.; Knoll, W. In preparation.

(37) Milner, S. T.; Witten, T. A.; Cates, M. E. *Macromolecules* **1988**, *21*, 2610.

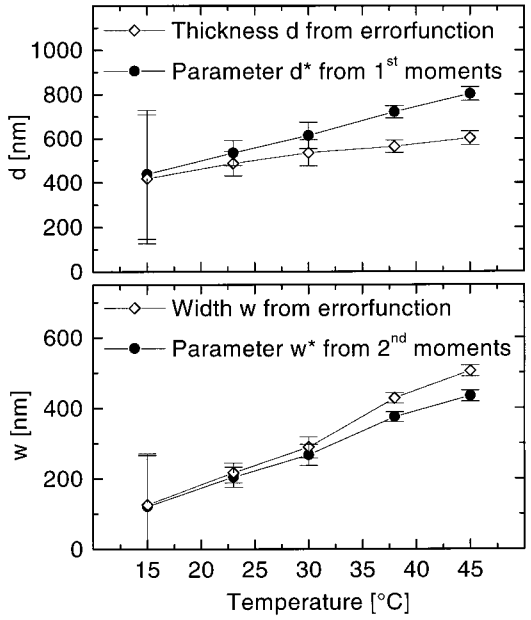

Figure 6. Brush thickness d and interface width w as obtained from fits with error functions and generalized thickness d^* and interface width w^* (see Appendix) calculated from the first and second moments of the segment density profiles.

Results and Discussion

Figure 4c shows the error function profiles that best fit the data for the various temperatures in cyclohexane. In Figure 6 the extracted parameters d and w are plotted as a function of temperature. For highly swollen brushes the profiles appears almost like exponentials. For these cases the parameter d in the error function is no longer a good measure of the brush thickness. d corresponds to the point of inflection and can even become negative. We have therefore defined model-independent parameters d^* and w^* which make use of the first and the second moment of the segment density distribution. The parameters d^* and w^* are defined independently of the error function but are numerically equal to the parameters d and w as long as w is much smaller than d. For large interface widths d^* and w^* are more suitable measures for thickness and interface width than d and w. The mathematics is given in the Appendix.

Figure 6 shows the thicknesses and interface widths corresponding to the best fits in Figure 3. Both the brush thickness and the interface width increase smoothly as a function of temperature, showing no abrupt variations around the θ temperature. Interestingly, the interface width appears to vary much stronger than the thickness.

Finally, we compare our findings to the results from Webber and co-workers[23] and to the mean-field calculations by Zhulina and co-workers.[15] The latter theory treats *monodisperse* brushes and can therefore not directly be compared to brushes with a polydispersity in the range of 2. Still, we consider this formalism as a starting point and a reference frame for discussion. The mean field theory predicts the thickness of a *monodisperse* brush at the θ condition H_θ as

$$H_\theta = \frac{4}{\pi}\left(\frac{w_3\, p}{2}\right)^{1/4}\left(\frac{\sigma}{a^2}\right)^{1/2} Na \qquad (2)$$

with H_θ the thickness at the θ temperature, w_3 the

dimensionless third virial coefficient, p a dimensionless parameter measuring the chain stiffness,[38] σ the area per chain, a^2 the area per monomer, and N the degree of polymerization. Webber and co-workers particularly focus their analysis on the normalized slope of the thickness $\mathrm{d}/\mathrm{d}T(\alpha) = \mathrm{d}/\mathrm{d}T(H/H_\theta)$. Close to the θ temperature the Zhulina theory predicts[23]

$$\frac{\mathrm{d}\alpha}{\mathrm{d}T} = \frac{v_0}{T_\theta}\frac{2}{3\pi}\left(\frac{p}{2}\right)^{1/4} w_3^{-3/4}\left(\frac{\sigma}{a^2}\right)^{1/2} \tag{3}$$

where we have used $v = v_0(T - T_\theta)/T_\theta$ for the excluded volume parameter v. The parameter v_0 is 0.516 for the PS/CH system.[39] For polystyrene we have $p \sim 1.7$. We have taken a as the cubic root of segment volume, which is about 5.5 Å. The third virial coefficient w_3 is derived from the relation $w_3 = 1/3 - \chi_1$, where $\chi_1 = 0.149$ describes the concentration dependence of the χ parameter according to $\chi \sim \chi_0 + \chi_1\varphi + ...$[40] This value is close to the value of $^1/_6$ used in ref 23. For a given thickness in the dry state the only free parameter is the degree of polymerization N. We chose N such that the thickness H_θ at the θ point matches the experimental value for d. The line of reasoning for the identification of H and d is that even for monodisperse brushes fluctuations generate an exponential tail of the segment density profile extending beyond H. The parabolic profile with an exponential tail actually looks quite similar to an error function. Setting $d \approx H$ seems the most natural choice. The derived molecular weight is about 10^6 g/mol, which is compatible with the gel permeation chromatography (GPC) data from the reference experiments (cf. Experimental Section). With this molecular weight the area per chain σ is fixed as is 11 nm^2, and the thermal expansion coefficient $\mathrm{d}\alpha/\mathrm{d}T$ ($T = T_\theta$) is 0.7%. The experimental value, on the other hand, is 2%. One can only speculate about the origin of the discrepancy. Polydispersity clearly is a strong candidate, because the calculations were done for monodisperse brushes. Milner and co-workers have calculated the segment density profiles of polydisperse brushes and find that the profiles are smoother than the ones found for the monodisperse case. In particular, the profile is no longer parabolic. Unfortunately, varying solvent quality is not addressed in this paper.

Interestingly, Webber and co-workers also find a thermal expansion coefficient larger than expected. Their values are 2.7%, 1.93%, and 0.95% for chain lengths of 444, 551, and 778 repeat units, respectively. They derive a prediction from the Zhulina theory in the range of 1%. The latter authors worked with rather monodisperse brushes obtained by anionic polymerization, which makes polydispersity an unlikely explanation. On the other hand, the grafting densities in their systems are so low that chain stretching is rather marginal. This is in conflict with the assumptions from the Zhulina theory. Also, it is not clear to us whether the results of a hydrodynamic experiment can be easily mapped onto the results of an ellipsometric measurement. Using a Brinkman-type approach to calculate the hydrodynamic thickness for error function profiles, we found that the hydrodynamic thickness strongly depends on the parameter w.[41] Assuming that the profiles become smoother at higher temperatures therefore could explain the high thermal expansion coefficient found for the hydrodynamic thickness. Webber et al. offer reversible adsorption of PS segments onto uncovered fractions of the substrate as an explanation for the high expansion coefficient. This argument can clearly not be applied to the systems studied here, because this kind of adsorption would only affect the first "blob" at the bottom of the brush, which is a tiny fraction of the entire system. Considering the considerable differences between the two experiments, we are not sure whether our findings and the results of Webber et al. have a common physical origin.

Conclusions

We have measured the thickness and the interface width of a polystyrene brush in cyclohexane with angle-dependent ellipsometry. The temperature dependent thickness and the interface width could be derived. As expected from mean field theory, the collapse proceeds continuously as a function of solvent quality. The interface width varies much stronger with temperature than the brush thickness.

Acknowledgment. We thank Alfons Becker for help with the determination of refractive indices.

Appendix: Generalized Thickness and Interface Width

We define the normalized first and second moment Z_1 and Z_2 of the segment density profile $\varphi(z)$ as

$$Z_1 = \frac{A_1}{A_0} = \frac{\int_0^\infty z\varphi(z)\,\mathrm{d}z}{\int_0^\infty \varphi(z)\,\mathrm{d}z} \tag{A1a}$$

$$Z_2 = \frac{A_2}{A_0} = \frac{\int_0^\infty z^2\varphi(z)\,\mathrm{d}z}{\int_0^\infty \varphi(z)\,\mathrm{d}z} \tag{A1b}$$

Z_1 and Z_2 have the dimensions of a length and the square of a length. To make the connection to the parameters d and w from the error function, we define the quantities

$$d^* = 2Z_1 \tag{A2a}$$

$$w^* = 2Z_1\sqrt{\frac{3}{2}\frac{Z_2}{Z_1^2} - 2} \tag{A2b}$$

In the following we show that for error functions with narrow interface width ($w \ll d$) the model-independent parameters d^* and w^* are equal to the parameters d and w. The nonnormalized moments A_0, A_1, and A_2 of the error function are given by

$$A_0 = \int_0^\infty \varphi(z)\,\mathrm{d}z = \int_0^\infty \frac{1}{2}\left(1 - \mathrm{erf}\left(\frac{z-d}{w}\right)\right)\mathrm{d}z$$
$$= \frac{1}{2}\left[\frac{\exp(-d^2/w^2)w}{\sqrt{\pi}} + d\left(1 + \mathrm{erf}\left(\frac{d}{w}\right)\right)\right] \tag{A3a}$$

(38) Fleer, G. J.; Cohen Stuart, M. A.; Scheutjens, J. M. H. M.; Cosgrove, T.; Vincent, B. *Polymers at Interfaces*; Chapman and Hall: Englewood Cliffs, NJ, 1993.

(39) Einaga, Y.; Ohashi, S.; Tong, Z.; Fujita, H. *Macromolecules* **1984**, *17*, 527.

(40) Gundert, F.; Wolf, B. A. In Brandrup, J., Immergut, E. H., Eds.; *Polymer Handbook*, 3rd ed.; Wiley: New York, 1989; p VII, 173.

(41) Domack, A.; Prucker, O.; Rühe, J.; Johannsmann, D. *Phys. Rev. E* **1997**, *56*, 680.

$$A_1 = \int_0^\infty z\varphi(z)\,dz = \int_0^\infty z\,\frac{1}{2}\left(1 - \mathrm{erf}\left(\frac{z-d}{w}\right)\right)dz$$

$$= \frac{1}{8}\left[\frac{2dw\,\exp(-d^2/w^2)}{\sqrt{\pi}} + (2d^2 + w^2)\left(1 + \mathrm{erf}\left(\frac{d}{w}\right)\right)\right] \quad \text{(A3b)}$$

$$A_2 = \int_0^\infty z^2\varphi(z)\,dz = \int_0^\infty z^2\,\frac{1}{2}\left(1 - \mathrm{erf}\left(\frac{z-d}{w}\right)\right)dz$$

$$= \frac{1}{12}\left[\frac{2w(d^2 + w^2)\,\exp(-d^2/w^2)}{\sqrt{\pi}} + (2d^3 + 3dw^2)\left(1 + \mathrm{erf}\left(\frac{d}{w}\right)\right)\right] \quad \text{(A3c)}$$

For $w \ll d$ the error functions in eqs A3 approach unity and the Gaussians vanish. This results in

$$A_0 \approx d$$

$$A_1 \approx \frac{d^2}{2} + \frac{w^2}{4}$$

$$A_2 \approx d\left(\frac{d^2}{3} + \frac{w^2}{2}\right) \quad \text{(A4)}$$

The moments Z_1 and Z_2 from eq A1 are

$$Z_1 = \frac{A_1}{A_0} \approx \frac{d}{2}\left(1 + \frac{1}{2}\frac{w^2}{d^2}\right)$$

$$Z_2 = \frac{A_2}{A_0} \approx \frac{d^2}{3}\left(1 + \frac{3}{2}\frac{w^2}{d^2}\right) \quad \text{(A5)}$$

In the limit of $w \ll d$ we find

$$d^* = 2Z_1 \approx d \quad \text{(A6a)}$$

$$w^* = 2Z_1\sqrt{\frac{3}{2}\frac{Z_2}{{Z_1}^2} - 2}$$

$$\approx d\sqrt{2\,\frac{1 + 3/2(w/d)^2}{1 + (w/d)^2} - 2}$$

$$\approx d\sqrt{2\left(1 + \frac{w^2}{2d^2}\right) - 2}$$

$$\approx w \quad \text{(A6b)}$$

LA980573D